https://doi.org/10.1016/j.compscitech.2023.109995

An embedded non-intrusive graphene/epoxy broadband nanocomposite sensor co-cured with GFRP for *in situ* structural health monitoring

Qingqing WANG[a, b, 1], Yuan TIAN[a,c, 1], Anchalee DUONGTHIPTHEWA[a], Jingzheng ZHANG[a], Menglong LIU[d, *], Zhongqing SU[b], Limin ZHOU[a, *]

[a]School of System Design and Intelligent Manufacturing, Southern University of Science and Technology, Shenzhen, 518055, PR China

[b]Department of Mechanical Engineering, The Hong Kong Polytechnic University, Kowloon, Hong Kong Special Administrative Region, PR China

[c]College of Aerospace and Civil Engineering, Harbin Engineering University, Harbin, 150001, PR China

[d]School of Mechanical Engineering and Automation, Harbin Institute of Technology, Shenzhen, 518055, PR China

Abstract

Glass fiber-reinforced polymer (GFRP) composites degrade continuously through service, entailing effective health monitoring to ensure structural integrity. We develop a new type of GFRP structure, with the embedded non-intrusive sensors for *in situ* structural health monitoring (SHM). Piezoresistive nanocomposite sensors – a pre-cured hybrid of graphene nanoplatelet (GNP) and epoxy, are molded in the second lamina of GFRP prepreg with epoxy matrix during lay-up to laminate process and then co-cured with GFRP composite, keeping the continuity at the interface between the composite. The GNP/epoxy sensor successfully captures the structural response from static strain to a high frequency ultrasonic wave up to 600 kHz with a gauge factor up to 26, which is the first ever nonintrusive GNP/epoxy piezoresistive sensor with an ultra-wide frequency response to mechanical deformation. Furthermore, the mechanical properties of host composite show negligible signs of

* Corresponding author.

[1] Qingqing Wang and Yuan Tian contribute equally to the article

E-mail address: zhoulm@sustech.edu.cn (L. Zhou), liumenglong@hit.edu.cn (M. Liu)

intrusion testified with tensile and bending tests. GFRP with embedded sensor features merits of high strength from GFRP as well as high-sensitivity sensing capability from the nanocomposite sensors, opening up a new avenue to *in situ* health monitoring of composites.

Keywords: A. Glass fibers; A. Nano composites; B. Sensing; D. Ultrasonic testing.

1. Introduction

With the benefit of design flexibility and excellent mechanical properties, fiber-reinforced polymer (FRP) composites have been extensively used in many crucial engineering applications such as aerospace, marine, wind turbine blades, civil, and automobiles [1-4]. FRPs are often used for load-bearing components due to their ability to withstand prolonged overload and thus prone to failure [4]. Once the composite material fails, the normal and orderly work of the entire system is affected, which, in severe cases, may cause irreversible loss of human and financial resources [5]. Therefore, online and *in situ* monitoring of the system status and estimating the system's life have become a vital part of the design and construction of composite structures. To fulfill the composite SHM, various sensors have been developed, such as optical fiber sensors [6], metal foil piezoresistive sensors (e.g. strain gauge) [7, 8], and piezoelectric sensors [9].

In addition to the sensor development, the mounting techniques to integrate the sensor and the host structure are of great significance to fulfilling a robust SHM of composite. Between the two common mounting methods, surface mounting is dominantly adopted over the embedded mounting, attributed to its convenient installing, disassembling, replacing, and maintaining. However, as the sensors are adhesively mounted on the surface of composite, they may be exposed to the harsh environment. Consequently, it is prone to the failure caused by chemical corrosion and external impact. Likewise, sensors may be difficult to paste on complex curved surfaces, and they are easy to detach under severe conditions and long-term working periods. Additionally, the relative movement between the sensor and the measured part is another crucial factor leading to inaccurate sensing and measurement [9-11].

In contrast to the surface mounting, embedded mounting in the composite structure helps protect

sensors and wires [12, 13], so the stability and life of the sensor are much less affected by the harsh environment. In addition, since the embedded sensor is in close contact with the structure, it is more stable than the surface mounting over the long-term monitoring process. Therefore, the functional integration of sensor into the composite materials has received widespread attention for SHM in composites. Researchers [13-15] have reported that embedded PZT into the composite structure can monitor the health of the structure in real-time. Comparing the embedded and surface-mounted sensors, the embedded PZT sensor structure is more sensitive and accurate for sensing wave motion [13-15]. However, as PZT is inconsistent to the host structure in terms of the material stiffness, the stress concentration can easily occur at the embedded position, affecting the performance and service life of the host structure [14, 16]. Fiber-optic sensors are often embedded in fiber-reinforced composite materials to monitor health conditions [17] because of the excellent characteristics of immunity to electromagnetic interference and light, durability, and high bandwidth [9]. However, a large diameter of fiber optic sensor (1 mm) will invade the host composite [17]. Although a smaller diameter (30-50 μm) is low intrusive, it is brittle and easily breaks [18] during the embedding and de-molding step [17]. Due to the high sensitivity, mechanical stability and flexibility of the strain gauges, it is always embedded in the FPR to monitor the curing process of the FPR. However, the poor compatibility of strain gauges and wires with epoxy resin may lead to delamination after fatigue loading at the embedded position of the strain gauge, thus affecting the life of the composite material [7]. As a result, PZT, fiber optic sensors, and strain gauges are not the best choices for embedded sensors for SHM.

Instead, the piezoresistive nanocomposite sensors [11, 19-22] recently became popular due to their higher sensitivities and flexibility compared with the conventional piezoresistive strain gauges. Many researchers [11, 20, 21, 23, 24] have done a lot of work on carbon-based nanocomposite film sensors for dynamic monitoring. The tunneling effect in the sensors plays a prominent role in sensing the mechanical response, when the distance of neighboring conductive nanoparticles (several nanometers) is close to the critical threshold. Around the critical threshold, even with an ultralow magnitude of

strain, the tunneling pathways in the sensor will be activated attributed to the distance change of the neighboring nanoparticles, resulting in considerable change of electrical resistance. Therefore, these sensors excel in sensing vibration and acoustic signals

Among various carbon-based nanofillers such as carbon nanotubes (CNTs) and carbon black for the nanocomposite sensors, the CNTs are easy to interwind with each other due to their large length-to-diameter ratio to form more contact paths between neighboring conductive nanoparticles, which diminishes the tunneling effect [25]. Similarly, the agglomeration of carbon black may impair sensor performance. With the special sheet structure, GNP has a greater probability of generating tunneling effect between adjacent graphene nanoplatelets. [11]. Thus graphene is becoming the most promising candidate for nanocomposite sensors due to its ability to form dense and conductive pathways at low nanofiller content. Many researchers have attempted to develop novel embedded graphene-based nanocomposite sensors. Nag-Chowdhury et al. [26, 27] fabricated strain-sensitive glass fiber reinforced polymer with graphene/epoxy deposited directly upon the whole glass fiber weaves and attached wire on the surface. With the sensor made with the same polymer (epoxy) as the glass fiber weaves, there is a tremendous improvement of both the gauge factor and the bonding with the glass fiber. But these sensors are only limited to quasi-static strain sensing. Su et al [22, 24] fabricated an implantable graphene/PVP sensor film, which offers wide measuring range from static to ultrasound. However, as the matrix of the developed nanocomposite is different from the matrix in the host structure in terms of the mechanical performance, the overall mechanical properties of the composite are compromised.

To overcome the aforementioned limitations of structural incompatibility between the embedded sensors and the host structure, this study creates a new fabrication method of embedded, compatible, and *in situ* sensors that are made with the same resin as the matrix for the host composite. The uncured GNP/epoxy nanocomposite sensors are printed in an interlayer of glass fiber prepregs and then co-cured with the prepregs, which is tested to realize a truly non-intrusive integration into the host structure with negligible degradation of mechanical performance. In addition, the study conducts an

ultrawide response test to evaluate the performances of the embedded co-curing GNP/epoxy sensor from static tensile, through vibration, to ultrasonic guided waves (UGWs) up to 600 kHz.

The rest of the paper is organized as follows. Section 2 elaborates on the fabrication of the GFPR with non-intrusive embedded sensor. In Section 3, the morphological, sensing and mechanical properties of the GFPR with the embedded sensor are analyzed through experimental results. Section 4 concludes a brief summary.

2. Experiment

2.1 Preparation of graphene/epoxy sensor

A sensor material preparation procedure was proposed to minimize nanofiller agglomeration and suppress the generation of void. Graphene (diameter: 50 μm, layers: < 3, and purity: > 95%) was supplied by TIME NANO Chengdu. Epoxy resin (Buehler® EpoKwick FC) was provided by BUEHLER USA. The fabrication procedure of GFRP composites with the embedded GNP/epoxy sensor is shown in Figure 1.

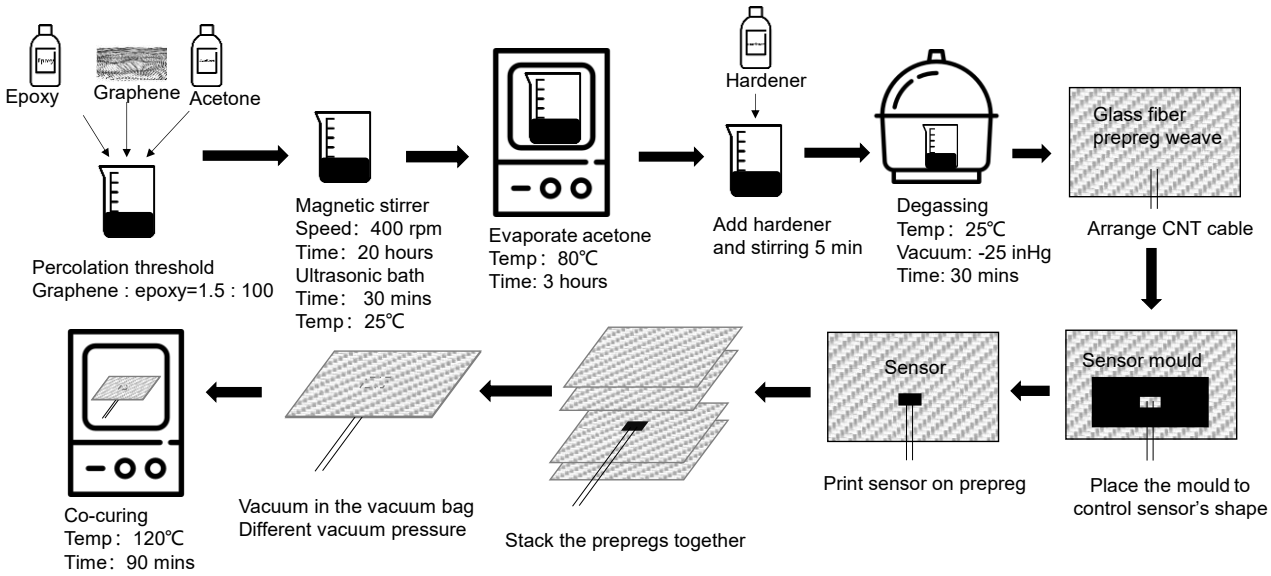

Figure 1. Flowchart of sensor and composite with sensor fabrication.

A total of 0.06 g of graphene nanofiller was dispersed in 4 g epoxy and then added to 4 ml acetone (purity: > 99.9%) to form a homogeneous dispersion using a magnetic stirrer at 25 ˚C with 400 rpm for 20 hours. Then, the mixture was sonicated in an ultrasonic bath for 30 mins, followed by acetone evaporation in a vacuum oven under -25 inHg at 80 ˚C for 3 hours. After the acetone was completely

evaporated, the hardener was added into graphene/epoxy using mechanical stirring for 5 mins, and then placed in the oven at a pressure of -25 inHg at 25 ˚C for 30 mins for degassing.

2.2 Fabrication of sensors and GFRP composites

Plain weave glass fiber prepregs with 38 wt% epoxy resin for GFRP composite were supplied by the Easycomposites UK. An electrical connection made of a carbon nanotube (CNT) fiber was purchased from TIME NANO. The glass plate was used as the baseplate, on all sides of which the release agent was coated and the sealant tape was pasted. The GFRP laminate consists of 4 layers of glass plain weave prepreg which was cut to the shape of the sample by a prepreg cutting machine (AOL® AOL-1313), and stacked on the baseplate. Then two CNT fibers as the connection wire were arranged in precise locations on the second glass fiber prepreg ply and the electrode distance between the two CNT fibers of each sensor was controlled at 1 mm. On the outside of the sample, the CNTs fibers are connected with metal cables through silver paint (shown in Figure S. 1). After that, the sensors with 1.5 wt% (closing to the percolation threshold [20, 23, 28] of graphene in the nanocomposite solution were printed at a specific position where the CNT fibers were fixed, and the initial thickness and shape of the sensor are controlled with a mold. After the sensor fills the mold, the mold was peeled off, followed by the stack of the remaining two prepreg plies. At last, the pill film, breather, and vacuum bag were placed in sequence on the top of the prepreg plies, as shown in Figure 2a.

After the above steps, sensors and prepregs were co-cured at 120 °C for 90 mins. To study the effect of co-curing fabrication pressure on the sensitivity of the sensor, GFRP composites with graphene/epoxy sensor and CNT fibers were fabricated at -15 inHg, -20 inHg, -25 inHg, and -30 inHg, namely GEP-15, GEP-20, GEP-25, and GEP-30, respectively. Note that -30 inHg equals the standard atmospheric pressure, which is the maximum pressure that can be reached with the vacuum bag. The

GFRPs with the embedded GNP/epoxy sensor fabricated at these four pressures are displayed in Figure 2b, showing different final shapes of this sensor. The spread of the embedded sensor to the nearby area increases as the pressure increases. Further, the fabrication pressure also influences the initial resistance and thickness of the embedded GNP/epoxy sensor. The average resistance of the embedded GNP/epoxy sensor fabricated at -15 inHg, -20 inHg, -25 inHg and -30 inHg are approximately 800 KΩ, 1 MΩ, 3 MΩ and out of the measurement range of the multimeter (> 1 GΩ), respectively. And the thicknesses of the sensors using a micrometer to measure (shown in Figure S. 2 in supplementary information for measurement method) is 105 μm, 76 μm, 62 μm, and 40 μm at -15 inHg, -20 inHg, -25 inHg, and -30 inHg, respectively, and the thickness of GEP-15, GEP-20, GEP-25, and GEP-30 is 0.9 mm, 0.89 mm, 0.89 mm, and 0.88 mm, respectively.

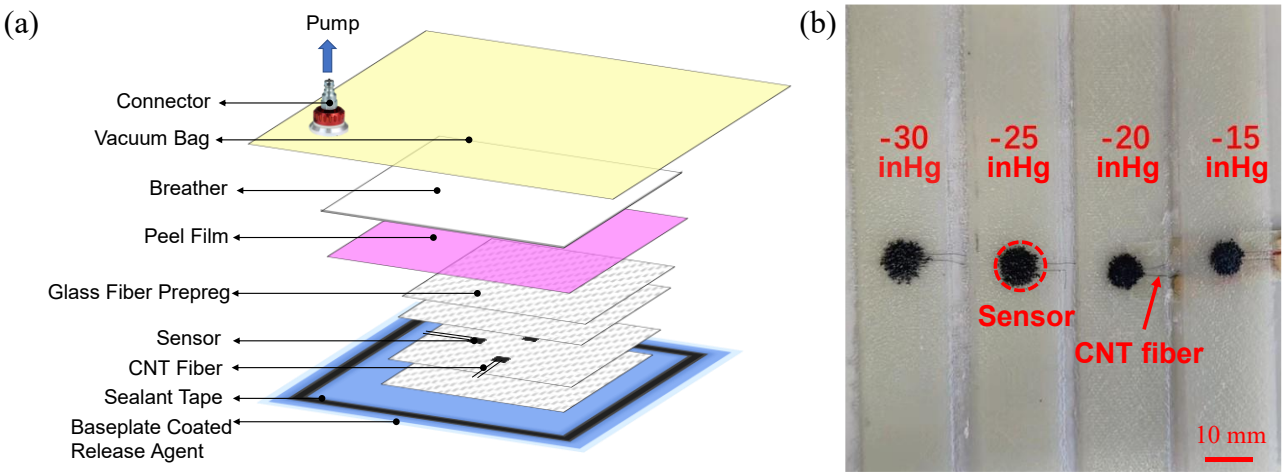

Figure 2. (a) The fabrication schematic of GFRP with embedded GNP/epoxy sensor, (b) the embedded sensor profile at different fabrication pressures.

3. Results and discussion

3.1 Morphological characterization of GFRP with embedded GNP/epoxy sensor

To explore the morphology of GFRP with GNP/epoxy sensors, two key factors need to be precisely observed, one is the graphene dispersion which determines whether the sensor has a strong sensing capability, and the other is the bonding condition that affects the mechanical performance of

the composite.

Before observing on a scanning electron microscopy (SEM) platform (FEI® Nova NanoSem450), the cross-section of the sample was first polished by a semi-automatic grinder polisher (Buehler® EcoMet 30) to gain a perfect surface, then a sputter coating was applied to each sample cross-section with a thin layer of gold, with some representative SEM images displayed in Figure 3. Figure 3a shows the cross-section of the GFRP with an embedded GNP/epoxy sensor. The sensor was integrated into the bonding interface located in the middle of GFRP. It is observed in Figure 3c that GNPs are dispersed randomly and evenly in an epoxy matrix. Because of the uniform dispersion, it is conducive to creating a stable conductive percolating network in the nanocomposite. And in Figure 3d at a smaller scale, a substantial number of tunneling paths built in the graphene network can be clearly observed, which is the precondition to trigger the tunneling current when subjected to external straining from quasi-static tensile, vibration, and GUWs, etc.

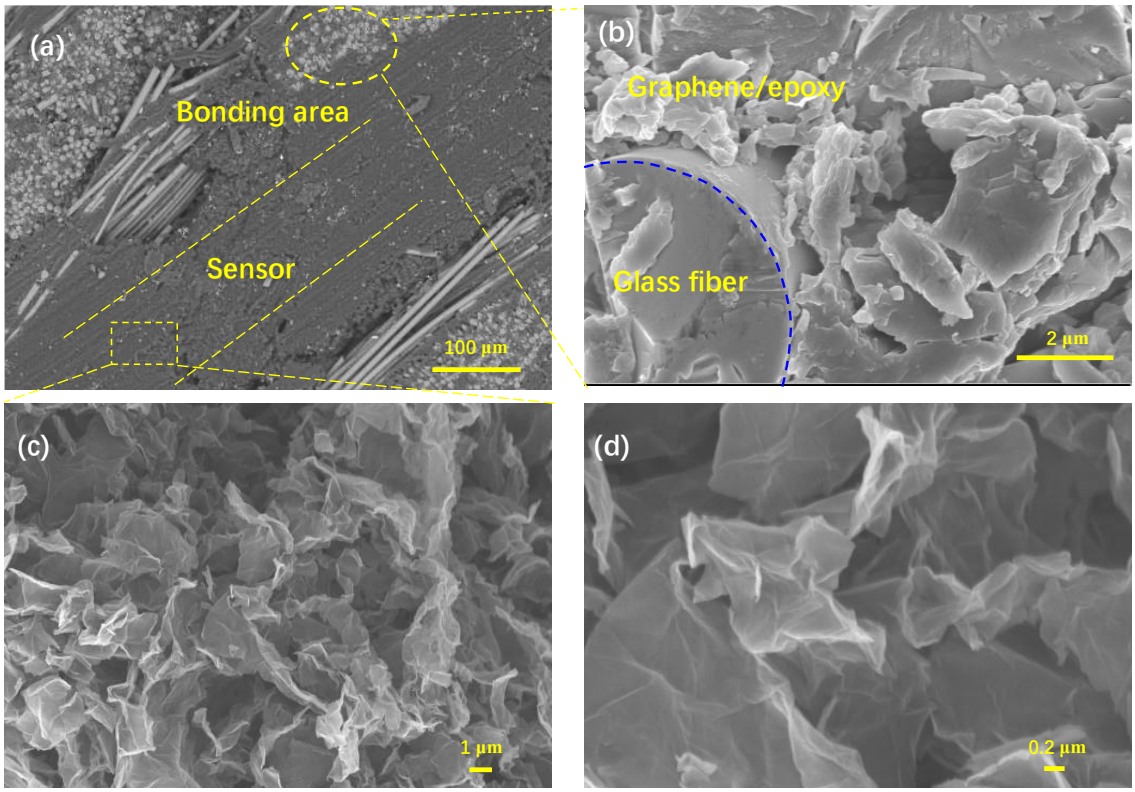

Figure 3. SEM images of (a) the cross-sectional GFRP laminate with an embedded sensor, (b) the interface between composite and embedded sensor, and (c, d) graphene/epoxy nanocomposite

sensor at two different scales.

As seen in Figure 3a, the sensor and glass fiber bundle are tightly bonded together to form a continuous whole in the area where the sensor is in contact with the glass fiber. And there is no visible interface between the GNP/epoxy sensor and composite matrix, the two are fused as a whole. A zoom-in of the GFRP where the embedded sensor is placed (see Figure 3b) further validates the tight sticking of the sensor material around the glass fiber, attributed to the identical matrix used for the nanocomposite sensor and the GFRP. Thus, the developed nanocomposite shows the potential of being truly non-intrusive to the host structure, while fulfilling the sensing capability, which are both validated in the following study.

3.2 Broadband sensing capabilities of GNP/epoxy sensor

To examine the sensing capabilities of the developed GNP/epoxy sensor to strains in a wide range of magnitude and frequency, the quasi-static tensile load, dynamic cycling load, vibration, and GUW tests were all conducted as follows.

3.2.1 Quasi-static test

The quasi-static tensile test of GFRP with sensor integration (250 mm × 25 mm) was performed to investigate the sensitivity of the sensor at different fabrication pressures. The changes in electrical resistance (ER) of the sensor were measured and recorded with a digital multimeter (Keithley® DMM7510) by the two point method as shown in Figure 4. The normal strain of the composites was measured with the extensometer. Gauge factor (K) can be defined by the relative change in electrical resistance due to a mechanical strain, which can be calculated as

$$K = \frac{\Delta R / R}{\Delta L / L} = \frac{\gamma}{\varepsilon_t}, \tag{1}$$

where ΔR is the change in ER, R is the initial resistance, ΔL is the change in length, L is the initial length, γ is the change ratio of ER, and ε_t is the tensile strain.

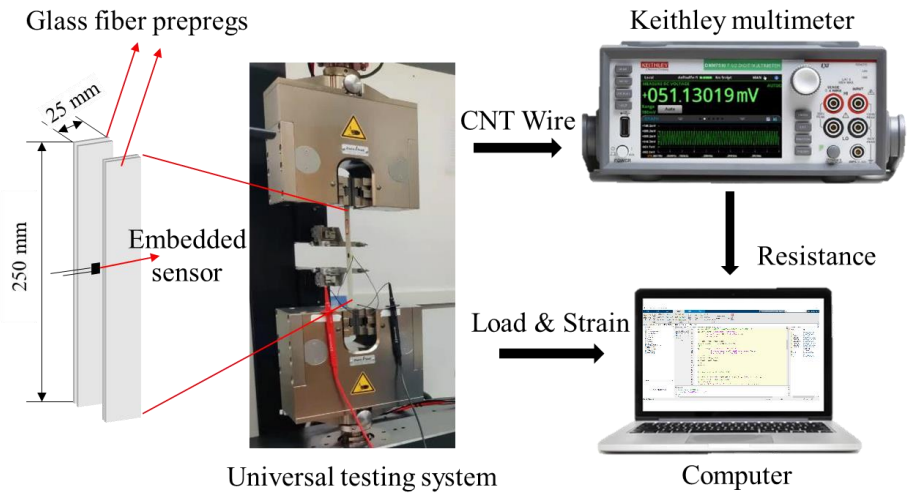

Figure 4. Experimental set-up of quasi-static test under tensile load.

The variation of gauge factor at different fabrication pressures is shown in a partial enlargement of Figure 5. Within the elastic domain ($\varepsilon_t < 0.3\%$), the fitted gauge factors of GEP-15, GEP-20, GEP-25 and GEP-30 are 20, 22, 26 and 0, respectively. In consequence of the nanocomposite sensor material being in an uncured state when evacuated in a vacuum bag, it is pressed to a certain thickness at specified pressure. The embedded sensor fabricated at lower pressures with larger thickness builds more conductive paths through the thickness than thin sensor. However, more conductive paths impair the sensitivity of strain, because the gap variation between adjacent GNPs is not sufficient to cause significant global resistance changes [26]. In addition, the embedded sensor fabricated at -30 inHg pressure does not exhibit any sensing capability. It is because that the embedded sensor is over-pressed and the GNPs are separated at -30 inHg pressure, which disrupts complete conduction path. As a result, at -25 inHg fabrication pressure, the gauge factor of the sensor is larger than those that of sensors at lower fabrication pressures, and 12 times larger than commercial strain gauges ($K = 2$).

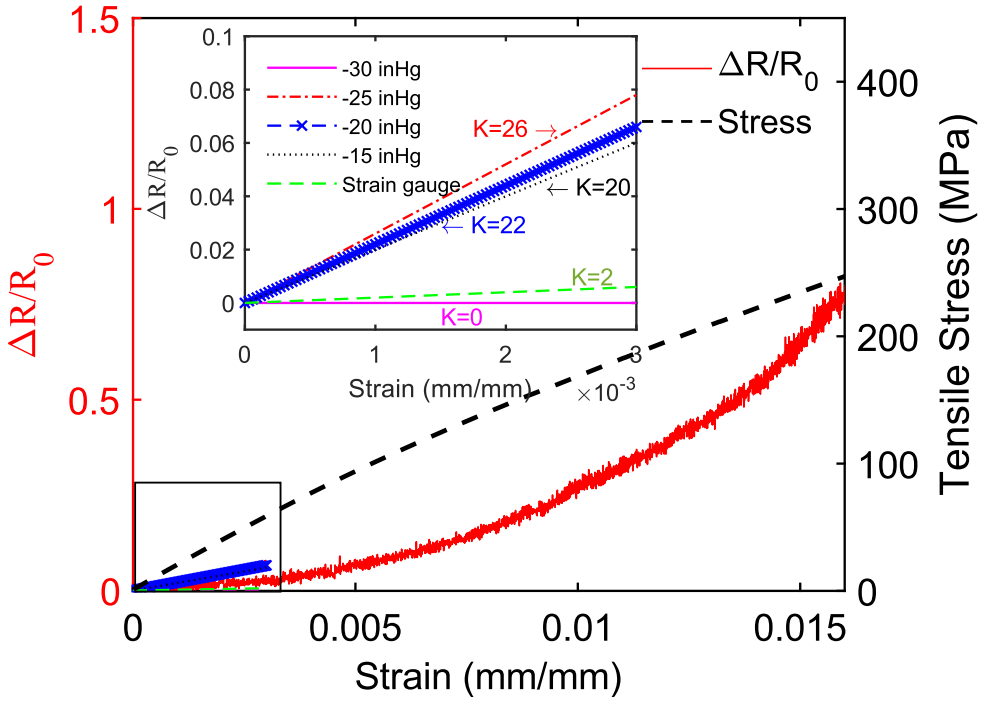

Figure 5. Stress-strain curve and relative change in ER of GEP-25 and the fitted gauge factor of the sensor at different fabrication pressures under elastic domain ($\varepsilon_t < 0.3\%$).

Figure 5 shows the relationship between relative change in ER and strain of GFRP with embedded GNP/epoxy sensor in the larger strain domain. The result shows that the tensile load induces strain resulting in positive increment in relative change in ER. And particularly the relative change in ER of GEP-25 presents a marked exponential growth. This exponential increase can be attributed to changes induced by tunnel resistance, which increases exponentially with distance from adjacent graphene nanoparticles, as confirmed by Moriche et al [28], leading to the formation of more tunneling paths. A large increase in the relative change in ER in the sensor at large strains leads rapidly to a rapid increase in gauge factor [26]. Therefore, different gauge factors of embedded sensor can be observed at different ranges of strain from Figure 5, which are around 26 (0-0.5%), 41 (0.5%-1%), 58 (1%-1.3%,), and 83 (1.3%-1.6%) for GEP-25, respectively. Hence, with the excellent strain sensitivity, GEP-25 is adopted for further dynamic testing.

3.2.2 Dynamic cycling test

The long-term sensing stability of the embedded GNP/epoxy sensor in GFRP was examined with cyclic tensile test. All the specimens were cycled at a constant strain range from 0 to 0.3%

(within the elastic domain) at a frequency of 0.1 Hz using LTM electrodynamic testing machine (ZwickRoell® linear testing system 10 kN).

As displayed in Figure 6, using a high-pass filter to filter out ambient noise, the ER change remains stable after 10000 cycles, indicating the good integrity of the conducting pathways in the developed sensor at quasi-static fatigue load. In order to observe the change of sensor resistance under a fatigue loading cycle, a few cycles (from 30 to 36 and 9970 to 9976) were selected to zoom in. As shown in Figure 6b, the ER change presents a slight decrease with the number of cycles increasing, which is corroborated in the reported works investigating fatigue in nanocomposites[29, 30]. That decrease could be associated to the relaxation of the polymer chains during a nanocomposite being cycled, thereby reducing the confinement of graphene nanofillers, causing the re-orientation of the nanofillers and the presence of stacked conductive particles or agglomerates.

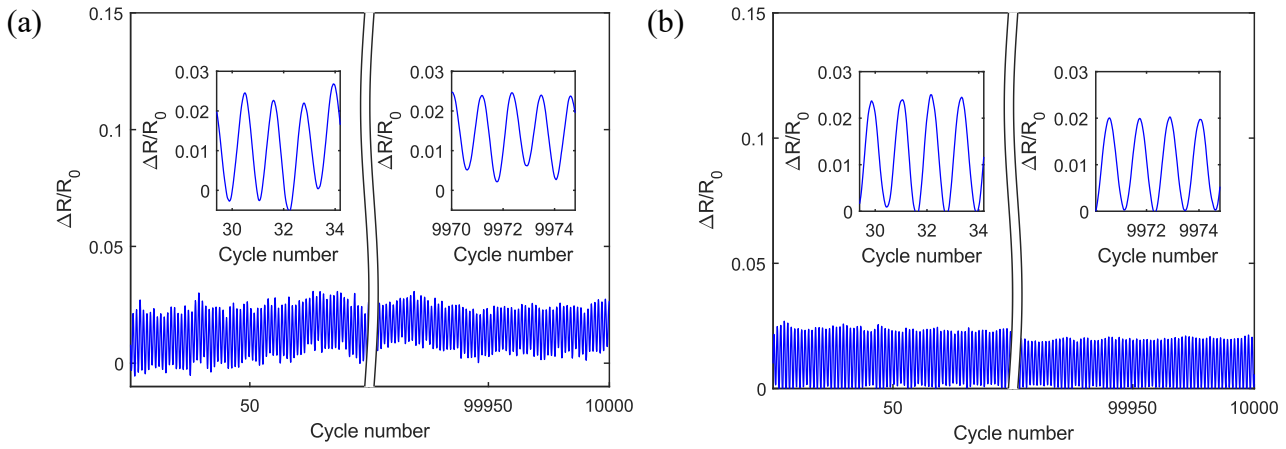

Figure 6. Raw (a) and filtered (b) change ratio of ER of GNP/epoxy sensor at 0.1 Hz cyclic fatigue load.

The ER change is also interrogated. As displayed in Figure 7, in the initial 1000 cycles, there is an increase of 3.3% in the ER of embedded sensor, after the remaining 9000 cycles, the ER slowly increases by 2%. This phenomenon is very common for composites loaded for the first time, i.e., the first 1000 cycles are to eliminate the prestress introduced by the preparation process. After the sensor was unloaded and stored statically for 30 days, the resistance of the sensor remains at the same value at the end of the fatigue experiment. It demonstrates that the microstructure of the embedded sensor slightly changes resulted from an irreversible change during cyclic loading. Because it is difficult to

completely remove the fine air bubbles in the sensor during the preparation process, which leads to crack propagation as the nanocomposite sensor undergoes cyclic tensile loading. Ultimately, this internal cracking leads to the destruction of part of the conductive network at the crack. With cycles from 875 to 880 (see Figure 6), the ER change exactly correlates with the applied load with no phase delay. The indicated quick response ability provides a potential for the sensor application to strains of higher frequency such as vibration and GUWs, which are tested as follows.

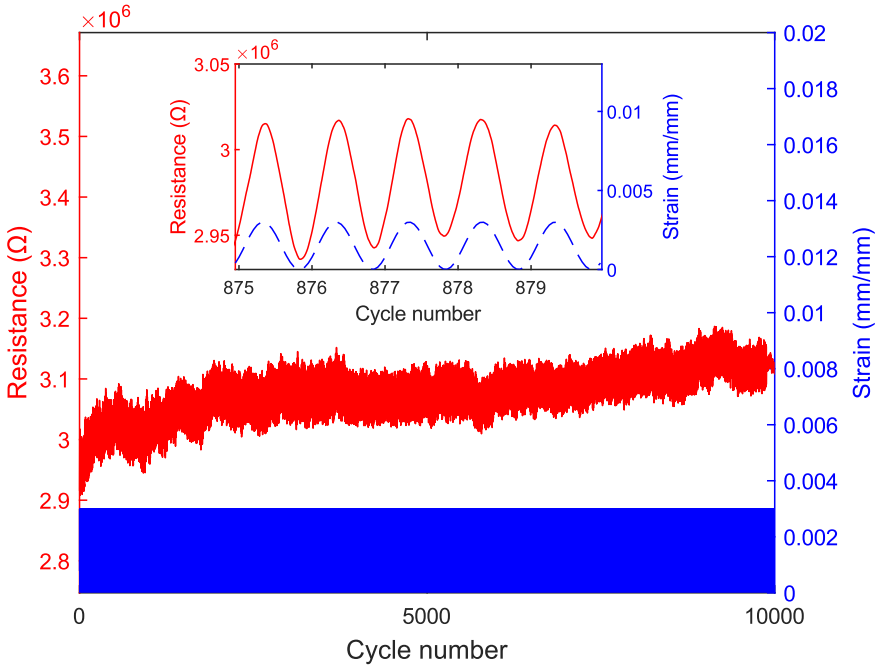

Figure 7. ER change of the embedded sensor at the cyclic strain of 0.3%.

3.2.3 Vibration test (300 Hz to 2 kHz)

After the quasi-static testing, the dynamic electromechanical response of the GFRP laminate (300 mm × 80 mm × 0.87 mm) with an embedded sensor was tested. The experimental platform is shown in Figure 8. One end of the laminate was clamped by a plain vice fixed on the bracket as a cantilever beam, while the other end was excited by the vibration machine. The excitations (from 300 Hz to 2 kHz) were generated by a waveform generator (Tektronix® AFG31051) through an electromechanical shaker system (SKC® YE-10) at 40 mm from the free end of a laminate. To calibrate the sensor performance, a strain gauge (350 Ω) was attached to the surface of the laminate at the same position as the sensor, which was 60 mm from the fixed end. The dynamic responses of the sensor and strain gauge were measured with a self-developed adjustable and commercial

acquisition system, respectively. The self-developed adjustable system integrates a Wheatstone bridge with adjustable resistors compatible with the ER of the developed sensor, which is powered by a power supply (ITECH® IT6302), and the commercial acquisition system (KYOWA® DPM-911B) was composed of a Wheatstone bridge and a signal conditioner. Then, both signals were input into an oscilloscope (Keysight® Infiniium MXR058A).

With a low magnitude of elastic disturbance from the vibration test, signals are prone to disturbance from the ambient noise and power radiation. Thus a band pass filter from 100 Hz to 5 kHz was applied to the raw signals. A sinusoidal vibration signal sweeping frequency test from 300 Hz to 2 kHz was performed, and the response signals are shown in Figure 9a. By observing the response signal, it is found that the sensor has a very good capability of dynamic stability, repeatability, and response reversibility, and the filtered signals show no waveform distortion or hysteresis. After that, a random frequency of 800 Hz is selected from the frequency sweeping to compare the response signal of the sensor and the strain gauge at this frequency as displayed in Figure 9b. Since two sensors are installed on opposite sides of the GFRP neutral axis (shown in Figure S. 3), the collected signals exhibit the differences in terms of both the magnitude and phase, but show the same frequency as the vibration excitation.

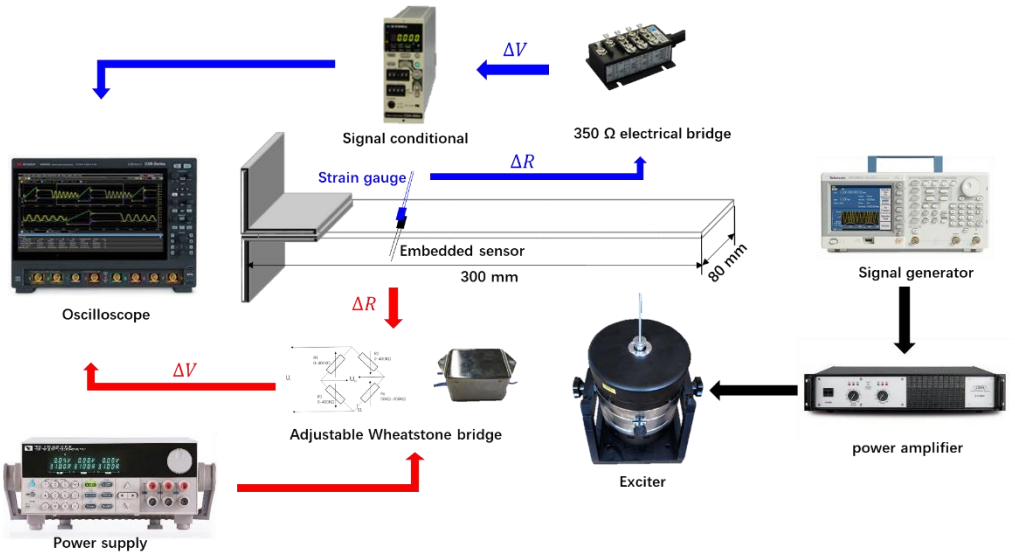

Figure 8. Experimental set-up of dynamic vibration test.

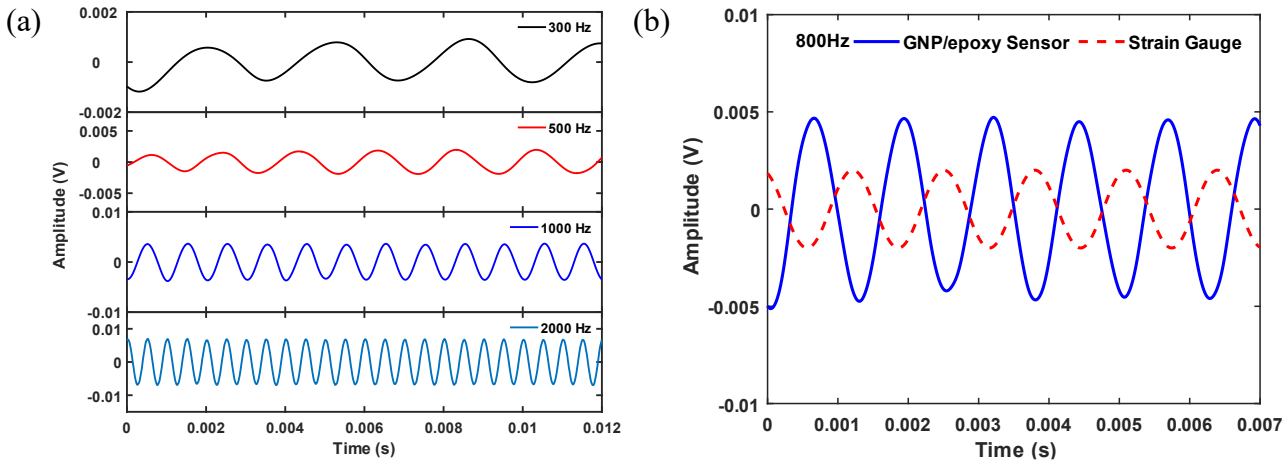

Figure 9. (a) Vibration response of GNP/epoxy sensor at different frequencies from 300 Hz to 2 kHz, and (b) response of GNP/epoxy sensor and strain gauge at 800 Hz.

3.2.4 Guided ultrasonic wave testing (150 kHz to 600 kHz)

Following the same fabrication process as detailed in Section 2, a GFRP (200 mm x 300 mm x 0.87 mm) with the embedded sensor was prepared, on which a PZT wafer (PSN-33, Ø10 mm, 1 mm thick) was surface mounted. A 3-cycle Hanning-window-modulated sinusoidal tone burst with the central frequency varying from 150 kHz to 600 kHz was generated by a waveform generator (Tektronix® AFG31051), and then amplified using a power amplifier (Falco systems® WMA-300) to a Vpp of 300 V to excite the PZT wafer. Another receiving PZT wafer was mounted on the surface where the GNP/epoxy sensor had been embedded, which is 150 mm from the excited PZT, to calibrate and compare the signal acquired with both sensors, as shown in Figure 10. For the developed nanocomposite sensor, the elastic disturbance-induced ER change was captured with a signal acquisition system, which consists of a self-developed adjustable amplification module and an oscilloscope. To suppress ambient noise and measurement uncertainties, the adjustable amplification module powered by a power supply (ITECH® IT6302) was developed, which is composed of a resistance-voltage transformation module converting piezoresistive variation to electrical signals, a bandpass filter, and a high-gain amplification module.

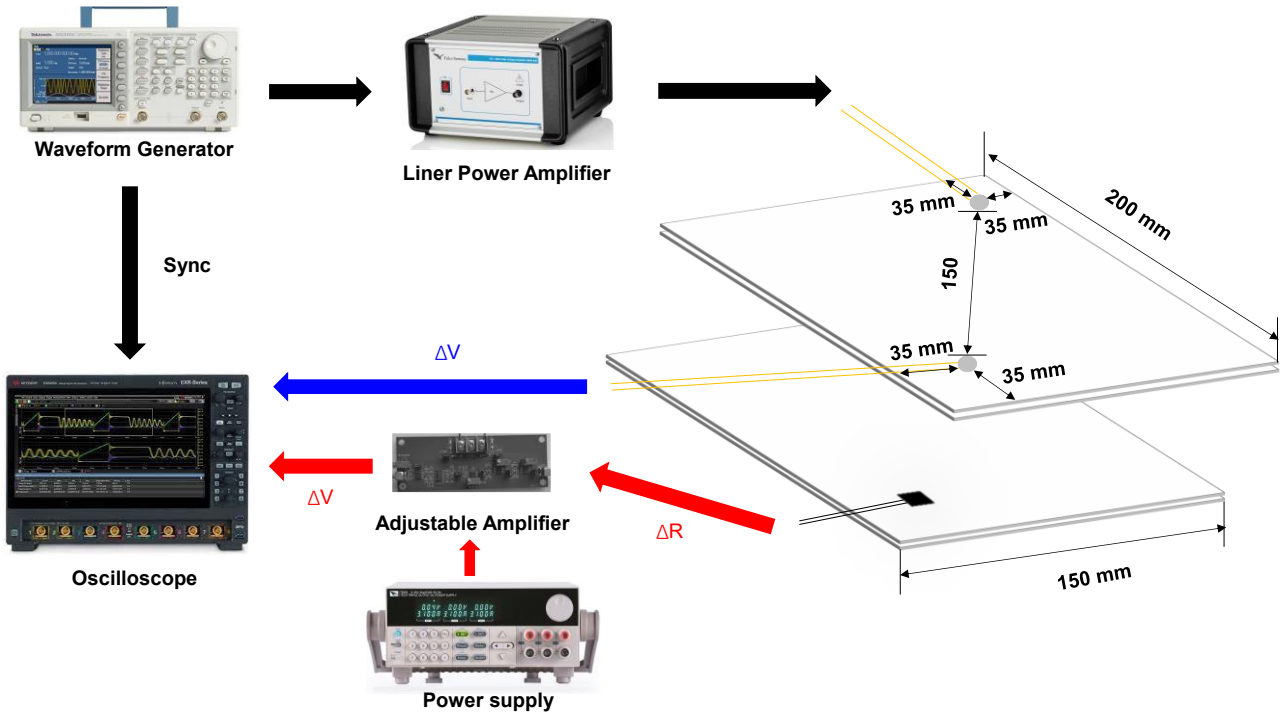

Figure 10. Experimental set-up of GUW test.

Figure 11 shows filtered ultrasonic signals acquired with GNP/epoxy sensor and PZT wafer between 150 kHz and 600 kHz. The qualitative coincidence in the time-of-flight of the first arrival zeroth-order symmetric Lamb wave (denoted by S_0) acquired with PZT and an embedded GNP/epoxy sensor for the wave modes is observed. Discrepancies in signal magnitude captured with the two types of sensors can be attributed to the distinct sensing mechanisms. The PZT wafer measures the changes in piezoelectricity, whereas the nanocomposite sensor measures the variation in piezoresistive properties based on the tunneling effect. To further investigate the sensing performances between 150 to 600 kHz (with a step of 30 kHz), the spectra of signals perceived with the GNP/epoxy sensor (see Figure 12a) and PZT wafer (see Figure 12b) are displayed over the time-frequency domain. Results show that the GNP/epoxy sensor exhibits a comparable sensing capability to a commercial PZT wafer. Thus, the embedded GNP/epoxy can be used to monitor the health condition of composite structures.

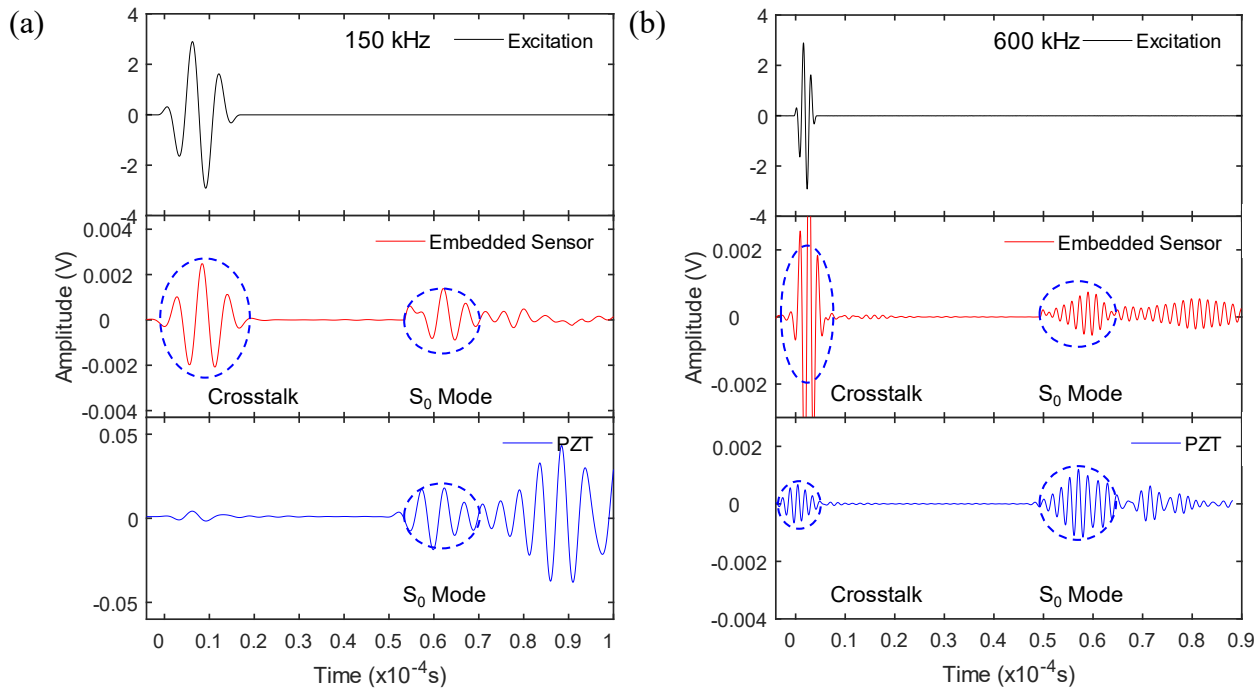

Figure 11. GUW signals acquired with the embedded GNP/epoxy sensor and surface-mounted PZT wafer at (a) 150 kHz, and (b) 600 kHz.

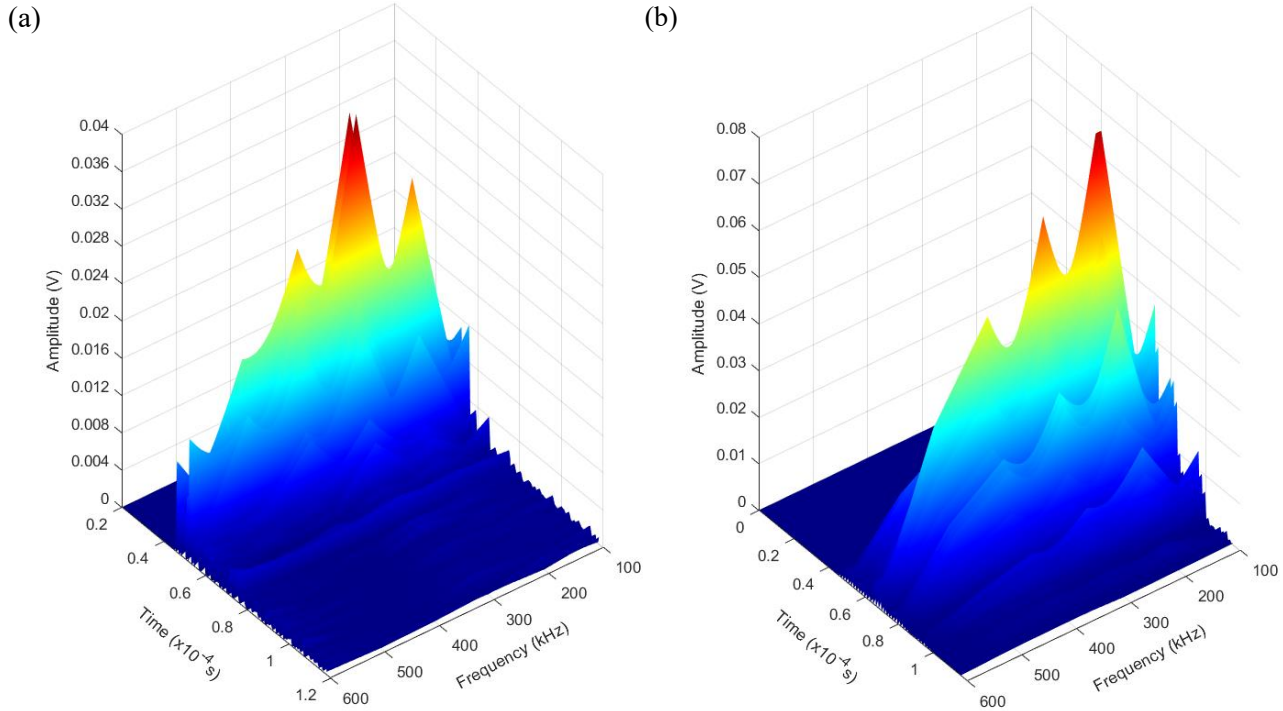

Figure 12. Time-frequency domain responses of (a) embedded GNP/epoxy sensor and (b) PZT wafer.

3.3 Mechanical properties of GFRP with embedded GNP/epoxy sensor

To study whether the developed GNP/epoxy sensor is mechanically compatible with composite structures, GEP-15, GEP-20, GEP-25, and GEP-30 were tested with the tensile and three-point

bending tests to investigate the effect of an embedded sensor on the mechanical properties of composites. The result of tensile properties and flexural properties are shown in Figure S. 4 and Figure S. 5, respectively, and the effect of embedded sensor is summarized in Table S. 1. Five samples were tested for each GFRP configuration. Since the gauge factor of GEP-25 is up to 26, which was selected for the series of test on sensing performance, the mechanical properties of GEP-25 will be elaborated next.

3.3.1 Tensile test

The tensile test was performed according to ASTM D3039 using a universal testing system (ZwickRoell® 20 kN Allround tabletop), as shown in Figure 13a. The GFRPs with and without an embedded sensor at the center of the composite are 250 mm × 25 mm × 0.89 mm in the in-plane dimension. To suppress the random errors, five samples were tested for each test. The raw dimension of the sensor before pressing is 4 mm × 4 mm. Glass fiber tabs were attached at two ends of the specimen with epoxy glue (3M® DP460) as reinforcing sheets to avoid breakage in the gripping area. The test was performed at a constant cross-head speed of 2 mm/min.

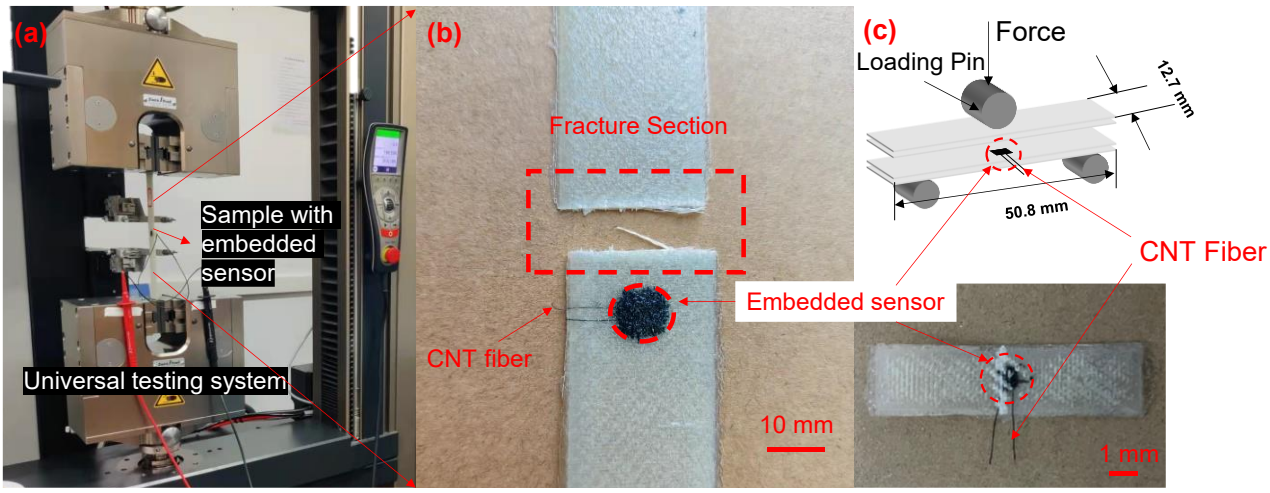

Figure 13. (a) Experimental setup of tensile test, (b) fracture of laminates with an embedded sensor, and (c) schematic diagram of three-point bending experiment.

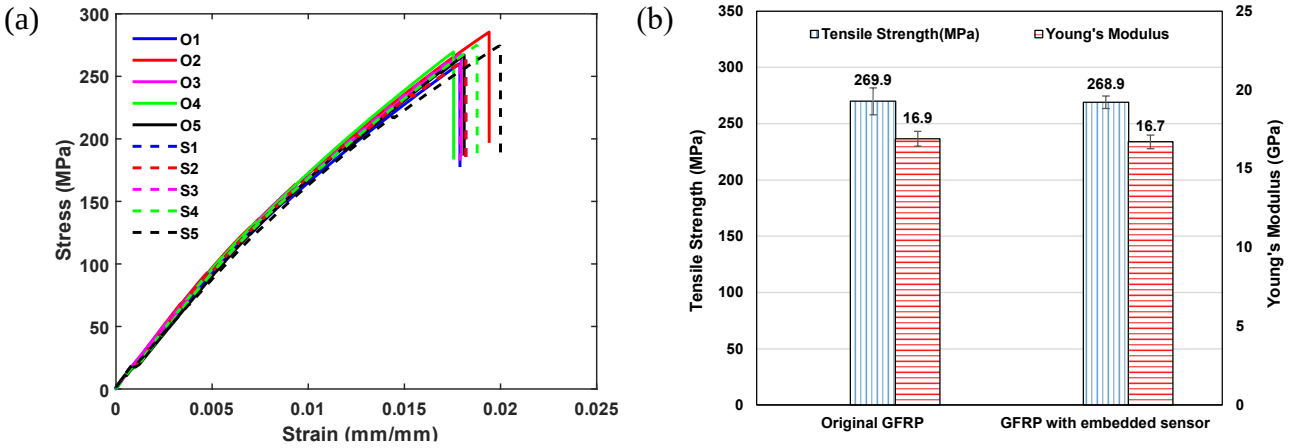

Figure 14. (a) Characteristic stress-strain curves (O1-O5: without embedded sensor; S1-S5: with embedded sensor) and (b) tensile modulus and strength of GFRP with and without sensor.

Figure 14 shows the result of GFRP with and without embedded sensor under tensile load. The stress-strain curve (in Figure 14a) for the GFRP composites with and without embedded sensor displays stress increasing gradually with applied tensile strain before reaching a brittle fracture. As displayed in Figure 13b, for all the five samples, the fracture occurs away from where the sensor was placed, which indicates the strong bonding between sensor and prepreg that withstands the tensile load.

Similarly, Figure 14b shows the comparison of tensile properties of composite with and without sensor. The tensile strength and Young's modulus of composite with embedded sensor are -0.3% and -1% less than the original GFRP, respectively, and this subtle difference comes from discrepancy in sample manufacturing and testing. Thus, the integration of the sensor, made of the same polymer as the host structure, shows almost the same mechanical property as the original host GFRP.

3.3.2 Three-point bending test

Following the above tensile test, the bending performance between the GFRP with and without the embedded sensor was further tested with the three-point bending test, which was performed using the universal test platform (WANCE TEST® TSE503A) with the speed of crosshead of 1 mm/min. Five respective GFRP samples (50.8 mm × 12.7 mm × 0.89 mm) with and without an embedded

sensor (2 mm × 2 mm) were prepared according to ASTM D790. To validate the influence of the embedded sensor on the bending performance, the cross section where the sensor is embedded is placed in the middle point of the test platform which withstands the largest bending moment, as shown in Figure 13c.

As displayed in Figure 15, compared with the original GFRP with the flexural strength and modulus of 412.5 MPa and 13.1 GPa, respectively, the GFRP with embedded sensor shows a slightly increase by 2.7% and 5.1%, respectively, attributed to the slight increase of thickness in the interply layer from the embedded GNP/epoxy sensor.

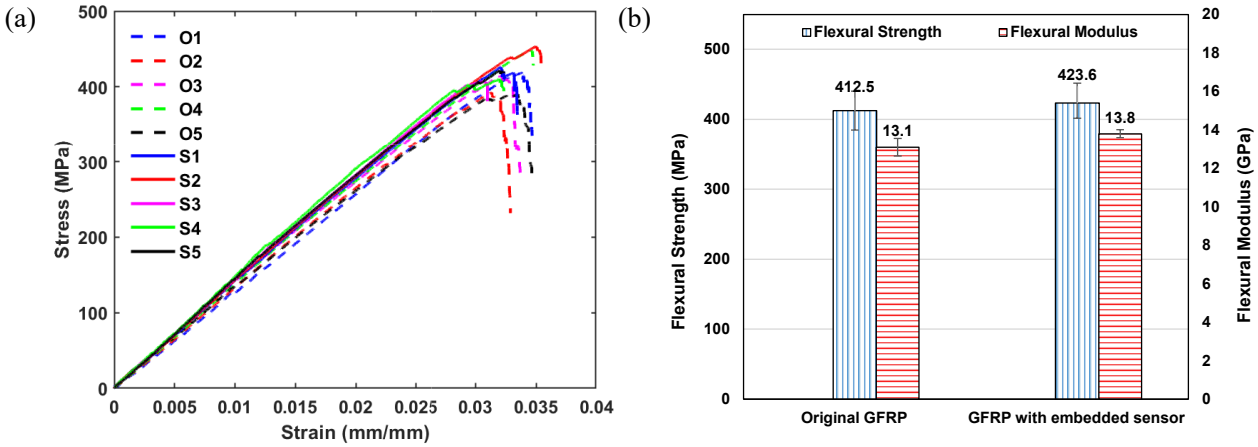

Figure 15. (a) Characteristic stress-strain curves (O1-O5: without embedded sensor; S1-S5: with embedded sensor) and (b) flexural modulus and strength of GFRP with and without sensor.

4. Conclusions

A nonintrusive GNP/epoxy nanocomposite sensor embedded into GFRP was developed. In an uncured state, the sensor is embedded in the specific prepreg layer during lay-up to laminate and then co-cured with GFRP composite. As observed from nanoscale morphological characterization, a remarkably reduced intrusion to the composites compared with conventionally embedded sensors is that this sensor with identical matrix of epoxy blends with prepreg's epoxy during curing process. Different pressures are applied to the co-curing process of GFRP with embedded sensors, whose gauge factors and mechanical performances at quasi-static tensile loading are found to reach a great balance at -25 inHg pressure. With the tested gauge factor up to 26 at -25 inHg pressure, the excellent

sensing capabilities of the developed sensor at cycling loading, vibration, and GUW up to 600 kHz are proved, exhibiting high stability, reversibility, and repeatability in responding to dynamic strains without phenomenal hysteresis and deviation. In addition, a series of tensile and bending tests prove that the GFRP composite's structural stiffness and strength are not adversely affected by the embedded sensor. Hence, GFRP composites with embedded sensor have both the inherent high mechanical properties from GFRP and the strain-sensing capabilities from sensor, which endows fiber-reinforced composites with potential for *in situ* health monitoring.

Declaration of competing interest

The authors declare that they have no known competing financial interests or personal relationships that could have appeared to influence the work reported in this paper.

Data availability

Data will be made available on request.

Acknowledgment

This research is supported by the National Natural Science Foundation of China (Grant No. 12072141 and 52105142), and Shenzhen Stable Support Grant (Grant No. GXWD20201230155427003-20200731161831019).

References

[1] S. Das, T. Yokozeki, A brief review of modified conductive carbon/glass fibre reinforced composites for structural applications: Lightning strike protection, electromagnetic shielding, and strain sensing, Composites Part C: Open Access 5 (2021) 100162.

[2] N. Forintos, T. Czigany, Multifunctional application of carbon fiber reinforced polymer composites: Electrical properties of the reinforcing carbon fibers - A short review, Composites Part B-Engineering 162 (2019) 331-343.

[3] M.A. Karatas, H. Gokkaya, A review on machinability of carbon fiber reinforced polymer (CFRP) and glass fiber reinforced polymer (GFRP) composite materials, Defence Technology 14(4) (2018) 318-326.

[4] T.P. Sathishkumar, S. Satheeshkumar, J. Naveen, Glass fiber-reinforced polymer composites - a review, Journal of Reinforced Plastics and Composites 33(13) (2014) 1258-1275.

[5] K. Diamanti, C. Soutis, Structural health monitoring techniques for aircraft composite structures, Progress in Aerospace Sciences 46(8) (2010) 342-352.

[6] B.W. Jang, C.G. Kim, Real-time detection of low-velocity impact-induced delamination onset in composite laminates for efficient management of structural health, Composites Part B-Engineering 123 (2017) 124-135.

[7] M. Kanerva, P. Antunes, E. Sarlin, O. Orell, J. Jokinen, M. Wallin, T. Brander, J. Vuorinen, Direct measurement of residual strains in CFRP-tungsten hybrids using embedded strain gauges, Materials & Design 127 (2017) 352-363.

[8] H.Y. Dong, H.M. Liu, A. Nishimura, Z.X. Wu, H.C. Zhang, Y.M. Han, T. Wang, Y.G. Wang, C.J. Huang, L.F. Li, Monitoring Strain Response of Epoxy Resin during Curing and Cooling Using an Embedded Strain Gauge, Sensors 21(1) (2021).

[9] H. Rocha, C. Semprimoschnig, J.P. Nunes, Sensors for process and structural health monitoring of aerospace composites: A review, Engineering Structures 237 (2021).

[10] M.H. Sherafat, R. Guitel, N. Quaegebeur, P. Hubert, L. Lessard, P. Masson, Structural health monitoring of a composite skin-stringer assembly using within-the-bond strategy of guided wave propagation, Materials & Design 90 (2016) 787-794.

[11] Y.Z. Liao, F. Duan, H.T. Zhang, Y. Lu, Z.H. Zeng, M.L. Liu, H. Xu, C. Gao, L.M. Zhou, H. Jin,

Z. Zhang, Z.Q. Su, Ultrafast response of spray-on nanocomposite piezoresistive sensors to broadband ultrasound, Carbon 143 (2019) 743-751.

[12] C. Tuloup, W. Harizi, Z. Aboura, Y. Meyer, K. Khellil, R. Lachat, On the use of in-situ piezoelectric sensors for the manufacturing and structural health monitoring of polymer-matrix composites: A literature review, Composite Structures 215 (2019) 127-149.

[13] J.S. Chilies, A.F. Koutsomitopoulou, A.J. Croxford, I.P. Bond, Monitoring cure and detecting damage in composites with inductively coupled embedded sensors, Composites Science and Technology 134 (2016) 81-88.

[14] X.L.P. Qing, S.J. Beard, A. Kumar, H.L. Chan, R. Ikegami, Advances in the development of built-in diagnostic system for filament wound composite structures, Composites Science and Technology 66(11-12) (2006) 1694-1702.

[15] S. Masmoudi, A. El Mahi, S. Turki, Fatigue behaviour and structural health monitoring by acoustic emission of E-glass/epoxy laminates with piezoelectric implant, Applied Acoustics 108 (2016) 50-58.

[16] X.P. Qing, S.J. Beard, A. Kumar, T.K. Ooi, F.K. Chang, Built-in sensor network for structural health monitoring of composite structure, Journal of Intelligent Material Systems and Structures 18(1) (2007) 39-49.

[17] L. Fazzi, S. Valvano, A. Alaimo, R.M. Groves, A simultaneous dual-parameter optical fibre single sensor embedded in a glass fibre/epoxy composite, Composite Structures 270 (2021).

[18] P.Y. Zhu, X.B. Xie, X.P. Sun, M.A. Soto, Distributed modular temperature-strain sensor based on optical fiber embedded in laminated composites, Composites Part B-Engineering 168 (2019) 267-273.

[19] Z.H. Zeng, M.L. Liu, H. Xu, Y.Z. Liao, F. Duan, L.M. Zhou, H. Jin, Z. Zhang, Z.Q. Su, Ultra-broadband frequency responsive sensor based on lightweight and flexible carbon nanostructured polymeric nanocomposites, Carbon 121 (2017) 490-501.

[20] Y.H. Li, K. Wang, Z.Q. Su, Dispersed Sensing Networks in Nano-Engineered Polymer Composites: From Static Strain Measurement to Ultrasonic Wave Acquisition, Sensors 18(5) (2018).

[21] P. Zhou, Y. Liao, Y. Li, D. Pan, W. Cao, X. Yang, F. Zou, L.-m. Zhou, Z. Zhang, Z. Su, An inkjet-printed, flexible, ultra-broadband nanocomposite film sensor for in-situ acquisition of high-frequency dynamic strains, Composites Part A: Applied Science and Manufacturing 125 (2019) 105554.

[22] Y.Y. Su, L. Xu, P.Y. Zhou, J.W. Yang, K. Wang, L.M. Zhou, Z.Q. Su, In situ cure monitoring and In-service impact localization of FRPs using Pre-implanted nanocomposite sensors, Composites Part a-Applied Science and Manufacturing 154 (2022).

[23] Y.H. Li, Y.Z. Liao, Z.Q. Su, Graphene-functionalized polymer composites for self-sensing of ultrasonic waves: An initiative towards "sensor-free" structural health monitoring, Composites Science and Technology 168 (2018) 203-213.

[24] Y.Y. Su, J.W. Yang, Y.Z. Liao, P.Y. Zhou, L. Xu, L.M. Zhou, Z.Q. Su, An implantable, compatible and networkable nanocomposite piezoresistive sensor for in situ acquisition of dynamic responses of CFRPs, Composites Science and Technology 208 (2021).

[25] Z.H. Zeng, M.L. Liu, H. Xu, W.J. Liu, Y.Z. Liao, H. Jin, L.M. Zhou, Z. Zhang, Z.Q. Su, A coatable, light-weight, fast-response nanocomposite sensor for the in situ acquisition of dynamic elastic disturbance: from structural vibration to ultrasonic waves, Smart Mater Struct 25(6) (2016).

[26] S. Nag-Chowdhury, H. Bellegou, I. Pillin, M. Castro, P. Longrais, J.F. Feller, Non-intrusive health monitoring of infused composites with embedded carbon quantum piezo-resistive sensors,

Composites Science and Technology 123 (2016) 286-294.

[27] B.R. Loyola, V. La Saponara, K.J. Loh, In situ strain monitoring of fiber-reinforced polymers using embedded piezoresistive nanocomposites, Journal of Materials Science 45(24) (2010) 6786-6798.

[28] R. Moriche, M. Sanchez, A. Jimenez-Suarez, S.G. Prolongo, A. Urena, Strain monitoring mechanisms of sensors based on the addition of graphene nanoplatelets into an epoxy matrix, Composites Science and Technology 123 (2016) 65-70.

[29] C.S. Boland, Quantifying the Contributing Factors toward Signal Fatigue in Nanocomposite Strain Sensors, ACS Applied Polymer Materials 2(8) (2020) 3474-3480.

[30] R. Moriche, M. Sanchez, S.G. Prolongo, A. Jimenez-Suarez, A. Urena, Reversible phenomena and failure localization in self-monitoring GNP/epoxy nanocomposites, Composite Structures 136 (2016) 101-105.